A Two-State Reactivity Rationale for Counterintuitive Axial Ligand Effects on the CH Activation Reactivity of Nonheme FeIVO Oxidants

ARTICLE *in* CHEMISTRY · FEBRUARY 2008

Impact Factor: 5.73 · DOI: 10.1002/chem.200701739 · Source: PubMed

4 AUTHORS, INCLUDING:

Lawrence Que
University of Minnesota Twin Cities
451 PUBLICATIONS **25,906** CITATIONS
SEE PROFILE

Sason Shaik
Hebrew University of Jerusalem
527 PUBLICATIONS **20,711** CITATIONS
SEE PROFILE

CHEMISTRY
A EUROPEAN JOURNAL

DOI: 10.1002/chem.200701739

A Two-State Reactivity Rationale for Counterintuitive Axial Ligand Effects on the C–H Activation Reactivity of Nonheme Fe^{IV}=O Oxidants

Hajime Hirao,[a] Lawrence Que, Jr.,[b] Wonwoo Nam,[c] and Sason Shaik*[a]

Abstract: This paper addresses the observation of counterintuitive reactivity patterns of iron–oxo reagents, $TMC(L)FeO^{2+,1+}$; $L = CH_3CN$, $CF_3CO_2^-$, N_3^-, and SR^-, in O-transfer to phosphines versus H-abstraction from, for example, 1,4-cyclohexadiene. Experiments show that *O-transfer reactivity correlates with the electrophilicity of the oxidant, but H-abstraction reactivity follows an opposite trend*. DFT/B3LYP calculations reveal that two-state reactivity (TSR) serves as a compelling rationale for these trends, whereby all reactions involve two adjacent spin-states of the iron(IV)–oxo species, triplet and quintet. The ground state triplet surface has high barriers, whereas the excited state quintet surface features lower ones. The barriers, on any single surface, are found to increase as the electrophilicity of $TMC(L)FeO^{2+,1+}$ decreases. Thus, the counterintuitive behavior of the H-abstraction reactions cannot be explained by considering the reactivity of only a single spin state but can be rationalized by a TSR model in which the reactions proceed on the two surfaces. Two TSR models are outlined: one is traditional involving a variable transmission coefficient for crossover from triplet to quintet, followed by quintet-state reactions; the other considers the net barrier as a blend of the triplet and quintet barriers. The blending coefficient (x), which estimates the triplet participation, increases as the quintet–triplet energy gap of the $TMC(L)FeO^{2+,1+}$ reagent increases, in the following order of L: $CH_3CN > CF_3CO_2^- > N_3^- > SR^-$. *The calculated barriers predict the dichotomic experimental trends and the counterintuitive behavior of the H-abstraction series.* The TSR approaches make a variety of testable predictions.

Keywords: C–H activation · density functional calculations · homogeneous catalysis · iron–oxo complexes · oxidation · two-state reactivity

Introduction

High-valent iron–oxo intermediates have long been implicated as the active species in oxidation processes of cytochromes P450 (P450s) and attracted considerable experimental and theoretical attention, in view of their versatile oxidative reactivity.[1–7] While the P450 iron–oxo species is still elusive, the situation is entirely different in nonheme iron biochemistry, where iron(IV)–oxo intermediates have now been trapped for three enzymes, taurine:α-ketoglutarate dioxygenase (TauD),[8–10] prolyl 4-hydroxylase,[11] and a halogenase CytC3.[12] Furthermore, a synthetic precedent for such iron–oxo species $[Fe^{IV}(O)TMC(NCCH_3)]^{2+}$ has also been characterized.[13–15] Besides structural and spectroscopic characterization, a wealth of reactivity data is rapidly accumulating that demonstrates the versatility of these reagents, which can perform a variety of transformations: alkane oxidation,[16–18] alcohol oxidation,[19,20] olefin epoxidation,[17,18,21] oxygen transfer to dialkylsulfides and trialkylphosphines,[13,18,21–26] and hydrogen abstraction from dihydroanthracene.[26–28] Interestingly, these complexes exhibit unusual kinetic isotope effect (KIE) patterns in H-abstraction reactions, ranging from near-classical KIE values of 10 for some reactions[26] to nonclassical values of 50–60 in others.[16,19,20] The fact that a large KIE value has been measured in the enzyme TauD[8] further enhances the allure of these reagents. The emerging reactivity features of these nonheme

[a] Dr. H. Hirao, Prof. S. Shaik
Department of Chemistry and the Lise Meitner-Minerva Center for Computational Quantum Chemistry
The Hebrew University of Jerusalem, 91904 Jerusalem (Israel)
Fax: (972) 2-658-4680
E-mail: sason@yfaat.ch.huji.ac.il

[b] Prof. L. Que, Jr.
Department of Chemistry and Center for Metals in Biocatalysis
University of Minnesota
Minneapolis, Minnesota 55455 (USA)

[c] Prof. W. Nam
Department of Chemistry
Division of Nano Sciences, and Center for Biomimetic Systems
Ewha Womans University, Seoul 120–750 (South Korea)

Supporting information for this article is available on the WWW under http://www.chemeurj.org/ or from the author.

iron–oxo species in the functionalization of C–H bonds thus present us a challenge to fashion a coherent model of reactivity.

One of the puzzles posed by the reactivity of the synthetic iron–oxo species is the intriguing effect of the axial ligand in a series of TMC(L)$FeO^{2+,1+}$ complexes, henceforth designated as $\mathbf{K_{TMC(L)}}$, in modulating the ability of the Fe^{IV}=O unit to effect C–H bond activation, a formally one-electron process, versus oxo-transfer to phosphorus, a formally two-electron process.[27,28] The $\mathbf{K_{TMC(L)}}$ series is the most systematically studied, where TMC is a tetradentate macrocyclic ligand (Scheme 1), and L is an axial ligand, which can be

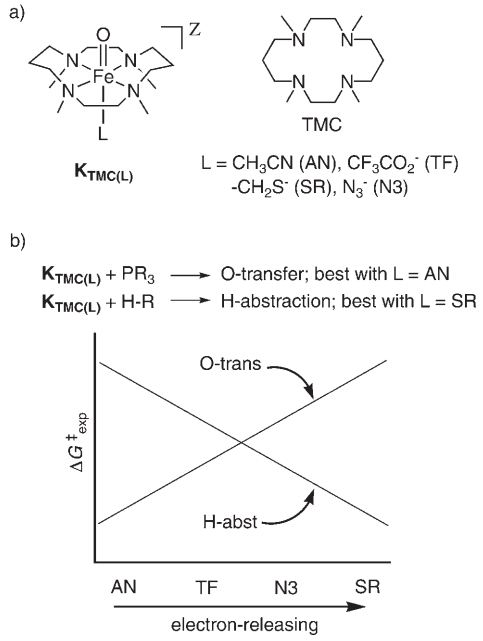

Scheme 1. a) TMC(L)Fe=O species ($\mathbf{K_{TMC(L)}}$) and b) a schematic representation of the observed trends in their two-electron and one-electron reactions.

neutral acetonitrile (AN) or monoanionic trifluoroacetate (TF), azide (N3), or thiolate (SR).[13,26–28] The anionic ligands are more electron-releasing than the neutral AN, and the most electron-releasing is SR in TMC(SR)FeO^{1+}, where the iron is ligated to a thiolate moiety that is tethered to the macrocycle.[28]

Preliminary reactivity comparisons between $\mathbf{K_{TMC(AN)}}$ and $\mathbf{K_{TMC(TF)}}$ revealed that $\mathbf{K_{TMC(TF)}}$ was more reactive towards H-abstraction from 9,10-dihydroanthracene compared with $\mathbf{K_{TMC(AN)}}$ at 25 °C, but similar in reactivity towards PPh_3.[27] Furthermore, $\mathbf{K_{TMC(SR)}}$ was found to be much more reactive towards 9,10-dihydroanthracene at −40 °C, but showed no reactivity towards PPh_3.[28] More recently, systematic studies[26] of an entire $\mathbf{K_{TMC(L)}}$ series demonstrated the opposing reactivity trends presented schematically in Scheme 1b, namely that the oxo-transfer (O-transfer) capability of $\mathbf{K_{TMC(L)}}$ towards PPh_3 increased in the order L = SR < N3 < TF < AN, but the reactivity in hydrogen-atom abstraction (H-abstraction) from 9,10-dihydroanthracene (DHA) decreased in the order L = SR > N3 > TF > AN. Thus the $\mathbf{K_{TMC(L)}}$ oxidant exhibits a dichotomic reactivity pattern: *in the oxo-transfer series it behaves as an electrophile, whereby electron-releasing ligands L diminish the oxidative reactivity, whereas in the C–H activation series it behaves in a contrarian manner, where electron-releasing ligands L surprisingly enhance the reactivity of the oxidant*. As such, a key question that needs to be addressed is: how can the oxidative capability of the obviously electrophilic $\mathbf{K_{TMC(L)}}$ oxidant be increased by an electron-donating axial ligand?

Since the factors governing these reactivity trends are not apparent from experiment,[26–28] the problem has to be addressed by means of theoretical calculations and modeling. Previous theoretical calculations of nonheme iron–oxo reactivity have revealed a few trends. In calculations of H-abstraction by triplet Fe^{IV}=O units, Decker and Solomon found $\mathbf{K_{TMC(AN)}}$ to be less reactive than the corresponding iron(IV)–oxo porphyrin complex.[29] Some of the present authors calculated the entire energy profiles for the reactions of $\mathbf{K_{TMC(AN)}}$ and $\mathbf{K_{TMC(TF)}}$ with cyclohexane, and found that the quintet surface cuts through the triplet-state energy surface, thus leading to a two-state reactivity (TSR) hypothesis.[30] More recently, de Visser studied hydroxylation and epoxidation of propene by $\mathbf{K_{TMC(SR)}}$, and compared this reactivity with those of a model of the iron(IV)–oxo species of TauD, as well as with Cpd I of cytochrome P450.[31] However, none of these theoretical studies addressed as yet the observed counterintuitive reactivity patterns of the $\mathbf{K_{TMC(L)}}$ series.[26–28] The goal of the work herein is therefore to understand this intriguing pattern and elucidate the effect of the axial ligand of $\mathbf{K_{TMC(L)}}$ on reactivity trends in the two series, to formulate a coherent and predictive reactivity model for nonheme iron–oxo reagents. To this end we studied with DFT methods the oxygen-transfer and hydrogen-abstraction reactions of the entire series of $\mathbf{K_{TMC(L)}}$ reagents (we added L = F^- and NCS^- to see how general the trends are) with PMe_3, PPh_3, and C_6H_8 (1,4-cyclohexadiene, CHD) (Scheme 2), and examined a few alternative models of reactivity.

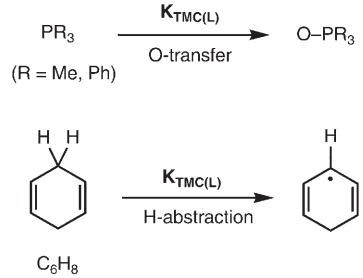

Scheme 2. Reactions studied in this paper. In addition to the $\mathbf{K_{TMC(L)}}$ species in Scheme 1 we added L = F^- (F) and NCS^- (NCS).

Computational Details

Procedures: All geometries were optimized with Jaguar 5.5[32] and Gaussian 03[33] at the UB3LYP/LACVP (UB3LYP/B1) level.[34,35] Geometries of local minima were

optimized with Jaguar 5.5. Transition-state (TS) geometries at the B3LYP/B1 level were initially optimized with Jaguar, and then located with Gaussian 03. We use this practice[36] since Gaussian has a more efficient frequency calculation module and gives more reliable energy values for TSs in some cases. The B3LYP/B1 geometry optimization was followed by frequency calculations by Gaussian 03 at the same level to characterize local minima and TSs. Zero-point vibrational energies (ZPEs) were also obtained by the frequency calculations. Molecular drawing was done in part with Molekel.[37]

Functionals: Since all the species involve two states, triplet and quintet, which are close in energy, we deemed it necessary to test along with B3LYP also the PBE0 functional;[38] the latter functional was found to be very successful in the prediction of the spin-state ordering in the $Fe(NH_3)_6^{2+}$ complex.[39a] Since the ground states of the $\mathbf{K_{TMC(L)}}$ reagents are known, we used these species to benchmark the two functionals. Considering that experimentally all the $\mathbf{K_{TMC(L)}}$ complexes have a triplet ground state, PBE0 was found to make poorer predictions than B3LYP, and for a given basis set PBE0 predicted many of the reagents to have a quintet ground state. It is important to point out that these complexes pose difficulties also to high-level configuration interaction methods, such as SORCI and CASPT2 based on large active spaces (e.g., CAS(20,13)), which predict quintet ground states even when the experimentally determined ground state is triplet.[39b,c] On the other hand, B3LYP gave results in general qualitative accord with experiment (see below), and was therefore employed as the standard method in the rest of the study. As expected, B3LYP*,[40] single-point calculations which were tried too, gave the same trends as B3LYP, while shifting the quintet state higher in energy, by several kcal mol^{-1}.

Basis sets: We used a few basis sets in the LACVP series,[35] which is implemented in Jaguar 5.5. The first one is LACVP, henceforth B1, which is a double-zeta valence basis set coupled with an effective core potential on Fe, and 6–31G on all other atoms. The other basis sets in the LACVP series are: LACV3P++** (B2), LACVP** (B3) and LACV3P (B4). These basis sets do not include polarization functions on Fe, such that, for example, LACV3P++** actually means a triple zeta with diffuse functions (LACV3P+) on Fe and 6–311++G** on all other atoms, etc. In addition to these LACVP-derived basis sets, we used the Stuttgart–Dresden relativistic ECP with a (8s7p6d1f)/[6s5p3d1f] valence basis set on Fe[41a] and 6–311++G** on all other atoms (B5), and finally, we also tested an all electron Wachters + f (14s11p6d3f)/[8s6p4d1f] basis set including a diffuse d function and a set of f polarization functions on Fe[41b,c] and cc-pVTZ on all other atoms (B6). These latter two basis sets carry f functions also on Fe. The performance of all the basis sets was examined by calculating the spin states of the $\mathbf{K_{TMC(L)}}$ reagents; the results were found to be very similar to B1.

Comments on the calculations of the spin states of $\mathbf{K_{TMC(L)}}$: As already noted, the triplet and quintet spin states of the $\mathbf{K_{TMC(L)}}$ reagents were calculated by single-point calculations with B3LYP, B3LYP* and PBE0 on the UB3LYP/B1 geometries, with the basis sets B2-B6 described above, hence UB3LYP/B*n*//B1 ($n=2$–6). B3LYP*/B1 and B3LYP*/B2 gave similar results to those of B3LYP, with somewhat larger gaps of spin states. All the results are tabulated in the Supporting Information (Tables SA1–SA2).

These many calculations demonstrated that B3LYP is superior to PBE0 for the cases at hand. Thus, for a given basis set, PBE0 predicts many of the reagents to have a quintet ground state, while the B3LYP/B1 and B3LYP/B3//B1 calculations predict correctly that all the $\mathbf{K_{TMC(L)}}$ reagents should possess a triplet ground state. All the larger basis sets, which include diffuse functions, predict that $\mathbf{K_{TMC(SR)}}$ should have a quintet ground state. However, Mössbauer studies show that the experimental data are inconsistent with a quintet ground state and fit well with a triplet ground state.[28] Despite this inconsistency, regarding the ground state, all sets of UB3LYP/B*n*//B1 and UPBE0/B*n* results for the triplet-quintet gap were found to correlate with one another (see Figure SA1 in the Supporting Information), thus indicating that the results are consistent, but involve a systematic error.

Calculations of energy profiles: Reaction pathways were verified by UB3LYP/B1 scan calculations along a given internuclear distance, while optimizing freely all other internal coordinates. The geometry at the top of the energy profile was used for subsequent optimization of the transition state. The C–H oxidation series was found to lead generally to a $C_6H_7^{\bullet}$ radical, which would rebound in a subsequent faster step, as found earlier.[30] However, since the interest here is in the rate-controlling C–H activation, we limited the study to the H-abstraction step. The basis set effect on TS geometry was tested using a B1 basis set augmented with polarization functions (B1′) on the immediate coordination sphere of Fe and on the phosphorous of PMe_3, hydrogen and carbon of the reacting C–H bond of C_6H_8. The effect on the transition states was not found to be sufficiently significant to warrant re-optimization of all the other species already characterized by B1 (see Figure SA4 in the Supporting Information). Therefore, the geometry optimizations of all other critical species were limited to UB3LYP/B1. In the reactions of $\mathbf{K_{TMC(AN)}}$, the gas phase potential energy profile of the quintet state descends in a barrier-free manner. Since this does not appear realistic for the reactions in solution, we scanned the energy profiles for the reactions of $^5\mathbf{K_{TMC(AN)}}$ in a solvent (acetonitrile; see below) and located the transition states with solvent effect taken into account. Since the numerical frequency analyses in solvent yielded, in addition to the reaction vector, a few low frequency imaginary modes, the transition state might be slightly deviant from the true transition state. However, multiple imaginary frequencies could also be due to the insufficient numerical ac-

curacy of numerical derivatives. Anyway the structure can be used as a good estimate of the transition state.

The energies of all the critical species were corrected by single point calculations with the larger basis set, B2, hence UB3LYP/B2//B1. Thus, even though the B1 and B3 basis sets appear to have the best results for the spin states of $\mathbf{K_{TMC(L)}}$, we preferred to carry out the single-point calculations with B2, since reaction barrier calculations in DFT require diffuse functions.[42] The energy was further corrected for the effect of acetonitrile ($\varepsilon = 37.5$, probe radius = 2.183 Å) by the self-consistent reaction field (SCRF) method implemented in Jaguar, using its own Poisson-Boltzmann solver.[43] In this method, the "solvation-phase energy" is defined as the sum of the gas-phase energy and the solvation energy (E_{solv}). The solvent corrections were done for the B1 as well as B2 basis sets. Although the solvent used in the experiment with $\mathbf{K_{TMC(SR)}}$ was methanol,[28] we used here acetonitrile in calculations as a common solvent for the sake of simplicity (and because the solvent effects were shown to be almost the same[26]). The trends in the B1 and B2 results are similar, and the respective data are summarized in the Supporting Information.

The free energies of activation, gauged relative to the separate reactants, are higher than the internal activation energies by an approximately constant quantity, for example, 11.3–13.0 kcal mol^{-1} on the triplet surface and on average 10 kcal mol^{-1} on the quintet surface (see Table SA4 in the Supporting Information). This quantity is dominated by the entropy contribution, due to the loss of rotational and translation degrees of freedom in the bimolecular process (see Tables SB9 and SC9 in the Supporting Information). Thus, when we present free energies these increments are added to the B2 data corrected by ZPE and free energy of solvation.

Calculations of kinetic isotope effects (KIEs): Following established procedures,[44] we calculated the semi-classical KIEs using the Eyring equation. Small corrections for the traditional tunneling mechanism through the barrier were applied by using the Wigner correction.[45]

Results

Spin states of $^{2S+1}\mathbf{K_{TMC(L)}}$: The $\mathbf{K_{TMC(L)}}$ complexes have two low-lying electronic states, singlet and quintet. The electron occupancies in the d-block orbitals of the triplet state of the $^3\mathbf{K_{TMC(L)}}$ species, possessing a $\delta^2\pi^*_{xz}{}^1\pi^*_{yz}{}^1$ configuration, are depicted in Scheme 3,[30,39b,c] while in the quintet state, the occupancy is $\delta^1\pi^*_{xz}{}^1\pi^*_{yz}{}^1\sigma^*_{xy}{}^1$, resulting from single-electron excitation of the triplet electrons from the doubly occupied δ orbital to the vacant σ^*_{xy}.

Figure 1 shows the structures of $^{3,5}\mathbf{K_{TMC(L)}}$ species optimized at the B3LYP/B1 level, along with the relative energies, which were calculated with and without ZPE and solvation corrections. Focusing on the geometric details in Figure 1 reveals a Fe–O distance of 1.65–1.68 Å for all complexes. $\mathbf{K_{TMC(SR)}}$ is seen to have the longest r(Fe–O) in the series of complexes studied here, implying a strong push effect of the axial ligand as is well known from the thiolate ligand effect in P450.[1,4,5] The r(Fe–N) value, which was calculated by taking the average of four distances between the iron and equatorial nitrogen atoms, exhibits a fairly large spin-state dependence; thus, in all species, r(Fe–N) was longest in the quintet state due to the occupation of σ^*_{xy}, as previously found in P450 compound I[46] as well as in several non-heme iron–oxo species.[30,39b,c,47] Another interesting feature is that the azide ligand (N3) coordinates to the iron center at an angle relative to the Fe=O axis, while the NCS ligand is collinear with this axis.

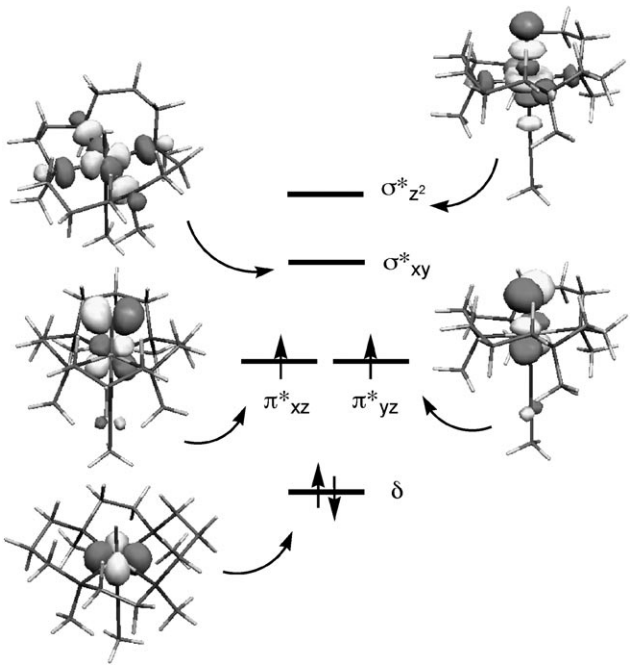

Scheme 3. Schematic illustration of orbital occupancies in the triplet state $^3\mathbf{K_{TMC(L)}}$ in the d-block orbitals.

Inspection of the relative energies of the spin states in Figure 1 reveals that the negatively charged ligands stabilize the quintet state relative to the triplet state. Thus, the triplet–quintet gap is largest for $\mathbf{K_{TMC(AN)}}$. At the UB3LYP/B1 level all the complexes possess a triplet ground state, but, at the UB3LYP/B2 level, both $\mathbf{K_{TMC(SR)}}$ and $\mathbf{K_{TMC(N3)}}$ are computed to have a quintet ground state, although both complexes were experimentally found to have triplet ground states.[23,28] Therefore, the B2 basis set, like other extended basis sets with more diffuse functions, appears to overestimate the relative stability of the quintet state (see also Tables SA1 and SA2 in the Supporting Information). B3LYP*/B2, on the other hand, gives triplet ground states for all species except $\mathbf{K_{TMC(SR)}}$. Interestingly, the solvent effect was found to be always larger for the triplet than for the quintet (Figure 1, and Table SA1 in the Supporting Information). These results qualitatively follow the relative dipole moments (see Table SA6 in the Supporting Information). In view of the basis-set dependency of the triplet–

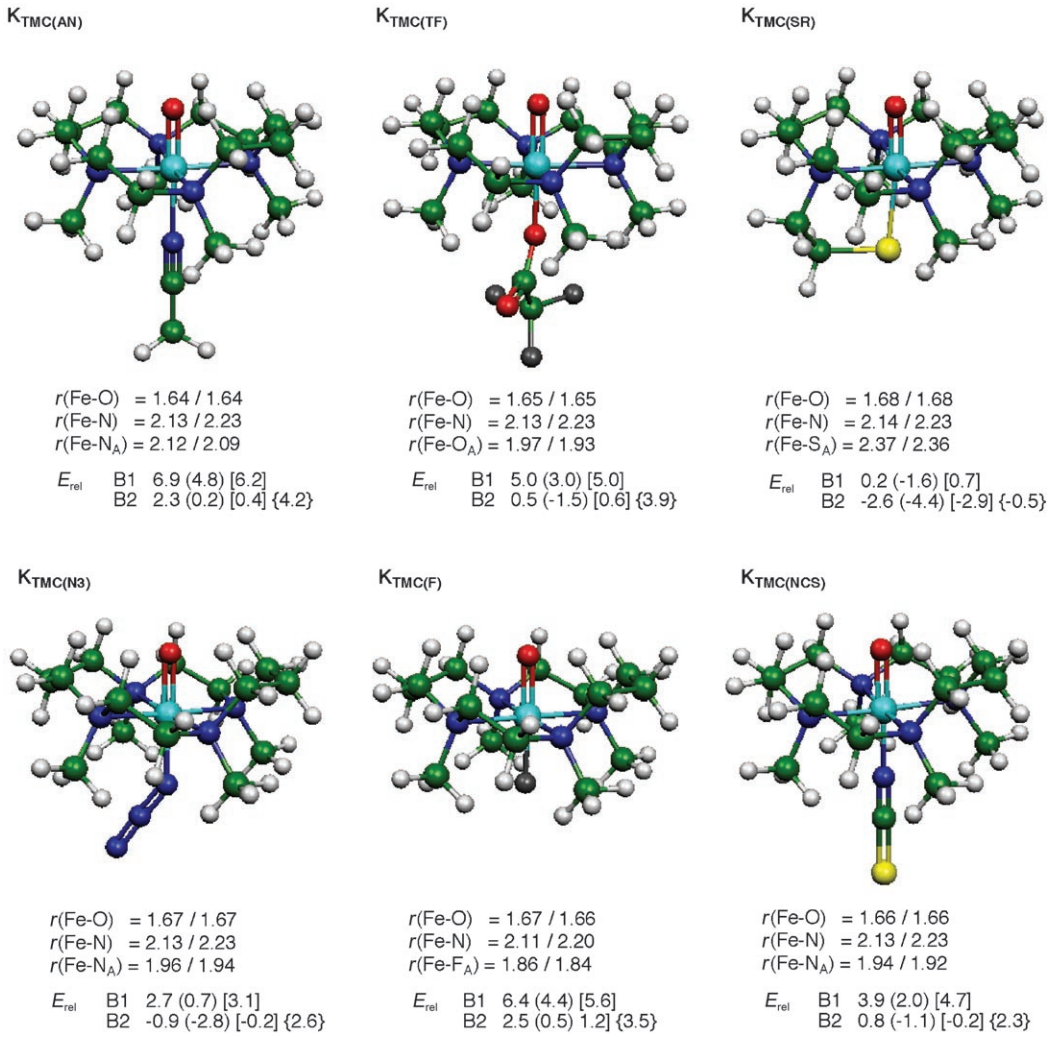

Figure 1. B3LYP/B1 optimized structures of $^{2S+1}\mathbf{K}_{\mathbf{TMC(L)}}$ complexes for the triplet/quintet spin states. The relative energies for the quintet states are given relative to the triplet state in the following order: E (E+ZPE) [E+ZPE+E_{solv}]. E(B3LYP*/B2)+ZPE(B3LYP/B1)+E_{solv}(B3LYP/B2) data are shown in curly braces.

quintet energy separation, two questions arise: a) what determines the triplet–quintet energy gap ΔE(Q−T) of $\mathbf{K}_{\mathbf{TMC(L)}}$?; b) do the B1, B$n$ (n=2–6) and other data correlate with each other? Let us answer these questions in turn.

Since the quintet state arises from the triplet by a promotion of one electron from the δ to the σ^*_{xy} orbital (Scheme 3),[30,39b,c] we plotted in Figure 2a the δ–σ^*_{xy} orbital energy gaps in the quintet state of $\mathbf{K}_{\mathbf{TMC(L)}}$ versus the ΔE-(Q−T) quantity (both at the B1 level). Figure 2b shows the relationship between the ΔE(Q−T) quantity and the charge transfer Δq_{CT} from the axial ligand L to the TMC–FeO^{2+} moiety (both at the B1 level). The charge transfer quantity Δq_{CT} is defined as the difference between the charge of the axial ligand L in its isolated state (0 or −1) and the Mulliken charge of L in $^5\mathbf{K}_{\mathbf{TMC(L)}}$.

Thus, Figure 2 shows the expected trend, namely that the quintet–triplet energy gap ΔE(Q−T) diminishes generally with an increase in the electron-releasing power of the axial ligand L and with the shrinkage of the δ–σ^*_{xy} orbital energy.[30,39b,c] To elucidate the factors that control the orbital energy gap, we computed the complexes with a point charge replacing the anionic ligand and placed at the same Fe–L distance as in the original complexes. The δ–σ^*_{xy} orbital energy gaps for cases tested (L=TF, N3) turned out to be virtually unaffected, or even slightly increased, due to the presence of a point charge (Figure SA10). As such, the charge placed at the site of the ligand L, away from the iron ion is not the origin of the orbital energy gap pattern in Figure 2a. However, in the presence of the actual ligand, some of the charge, originally on the ligand, is transferred (see Figure 2b) to the $TMCFeO^{2+}$ moiety and hence closer to iron, and this narrows the orbital gaps to an extent dependent on the donor capability of the ligand. Thus, as the amount of charge transferred from the axial ligand to the TMC–FeO^{2+} moiety gets larger, the δ orbital that is more concentrated on Fe gets destabilized relative to the more delocalized σ^*_{xy} orbital. Consequently, the orbital energy gap gets smaller, and hence ΔE(Q−T) decreases. The thiolate

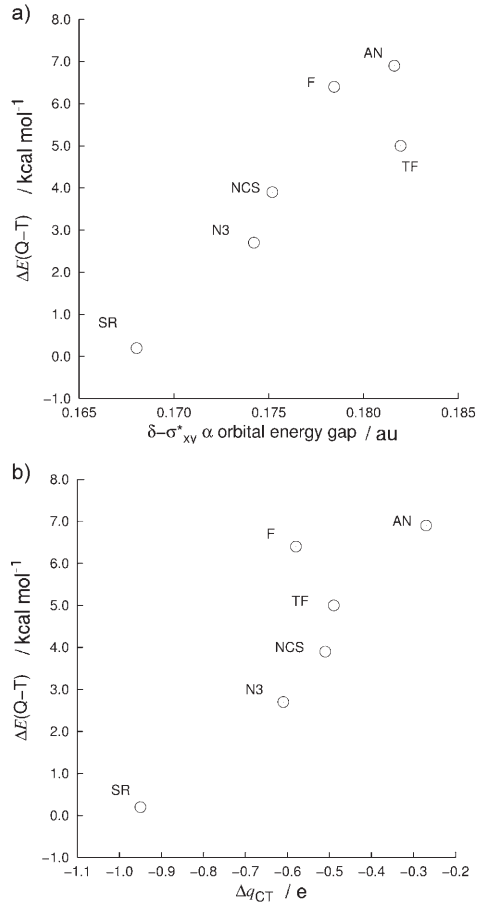

Figure 2. Relationships between a) δ–σ^*_{xy} orbital energy gap and ΔE(Q−T) and b) Δq_{CT} and ΔE(Q−T).

ligand has the strongest electron-donating ability (Figure 2b), and the gap was smallest in $\mathbf{K_{TMC(SR)}}$. The same correlations are obtained for other cases as well, except the cases of PBE0/B2//B3LYP/B1 and B3LYP/B5//B3LYP/B1, where unnatural Δq_{CT} values ($|\Delta q_{CT}| > 1.0$) were observed for some ligands and large deviations were obtained for L= TF and SR (see Figure SA2 in the Supporting Information). These deviations might reflect the numerical problem of the Mulliken charges with large basis sets. In the rest of the text we focus on the UB3LYP/B2//B1 data, mostly because we are interested in the relative barriers, and these quantities benefit from diffuse functions,[42] which are present in B2.

Oxygen transfer from $^{3,5}\mathbf{K_{TMC(L)}}$ to PMe_3 and PPh_3: Figure 3 shows the gas-phase energy profiles for the oxo-transfer reactions of $^{3,5}\mathbf{K_{TMC(AN)}}$ and $^{3,5}\mathbf{K_{TMC(TF)}}$ to PMe_3. The two cases cover the range of phenomena found for the various axial ligands excluding quantitative considerations. The gas-phase energy profiles in Figure 3a involve an initial cluster formation, $^{3,5}\mathbf{RC_O}$, between the reagent and the phosphine substrate, followed by a transition state, $^{3,5}\mathbf{TS_O}$, which leads to synchronous oxo-transfer, and by the formation of the ferrous-phosphine oxide product complexes, $^{3,5}\mathbf{P_O}$. As noted in a previous study of nonheme iron systems, here too, we encounter the same two-state reactivity (TSR) scenario[30] with a quintet state surface that is initially an excited state and then crosses through the triplet barrier, thereby providing in principle a low energy path for the process. Note in particular, how small the quintet barriers are compared with the triplet ones.

Figure 3b shows the energy profiles in a solvent where the TSR situation is maintained, but with some obvious changes. Thus, in solution the $\mathbf{RC_O}$ cluster is higher in energy than the separate reactants and the barriers increase compared with the gas-phase situation. As a result of these changes, we can presume that in solution there is no stable cluster (if at all), and we shall omit it from the considerations for all the reactions. Note that in a solvent a quintet transition state and barrier appear for L=AN. However, the quintet state barriers remain small even after solvation correction of the energies.

The study of O-transfer to PPh_3 was limited to L=AN, N3 and SR. Figure 4 shows the representative cases for L= AN and SR. The results in Figure 4 are similar to those in Figure 3, with the quantitative exception that, for a given $\mathbf{K_{TMC(L)}}$, the barriers for O-transfer to PPh_3 are larger than the corresponding ones towards PMe_3. Our calculations show that this trend is due to the solvent effect, which is mainly because of the larger solvation stabilization of the PPh_3 substrate (8.0 kcal mol^{-1} with B2, see Table SB12 in the Supporting Information) than that for PMe_3 (1.4 kcal mol^{-1} with B2, Table SB8 in the Supporting Information). Furthermore, much like for PMe_3, here too with the amendment of the overestimated quintet stability for L=SR and N3 (see Tables SB11 and SB12 in the Supporting Information), these reactions involve also TSR, with a higher triplet barrier and with a quintet state that cuts through the triplet surface.

As we saw above in Figure 3 with PMe_3, also here with PPh_3 in the gas phase, the quintet energy profile for L=AN exhibits a barrier-free process. Thus, the gas-phase $\mathbf{K_{TMC(AN)}}$ species is a superb electron acceptor (the gas-phase electron affinity of $\mathbf{K_{TMC(AN)}}$ is 197.8 kcal mol^{-1}[30]) and an electron transfer from PPh_3 to the iron–oxo reagent precedes the O-transfer (which thereby occurs in a barrierless fashion). However, in a solvent the electron affinity of $\mathbf{K_{TMC(AN)}}$ decreases to 95.1 kcal mol^{-1},[30] and the electron transfer is suppressed. The quintet energy profile in Figure 4 was therefore determined by scanning the energy in a solvent for internuclear separation of the $^5\mathbf{K_{TMC(AN)}}$ and PPh_3 in the range r(P–O)=3.4–2.7 Å (see Figure SB15 in the Supporting Information) prior to optimization of $^5\mathbf{TS_O}$ in solvent with Jaguar. The transition state species was characterized by its forces only and frequency analysis was not done due to high computational cost. Nevertheless, the scan and optimization calculations guarantee that this species has energy very close to that of the real transition state.

The transition state structures in Figure 5 show that P–O bond making and Fe–O bond breaking are generally more advanced for the triplet $^3\mathbf{TS_O}$ species (a late TS) than for the corresponding quintet $^5\mathbf{TS_O}$ species. For a given spin state,

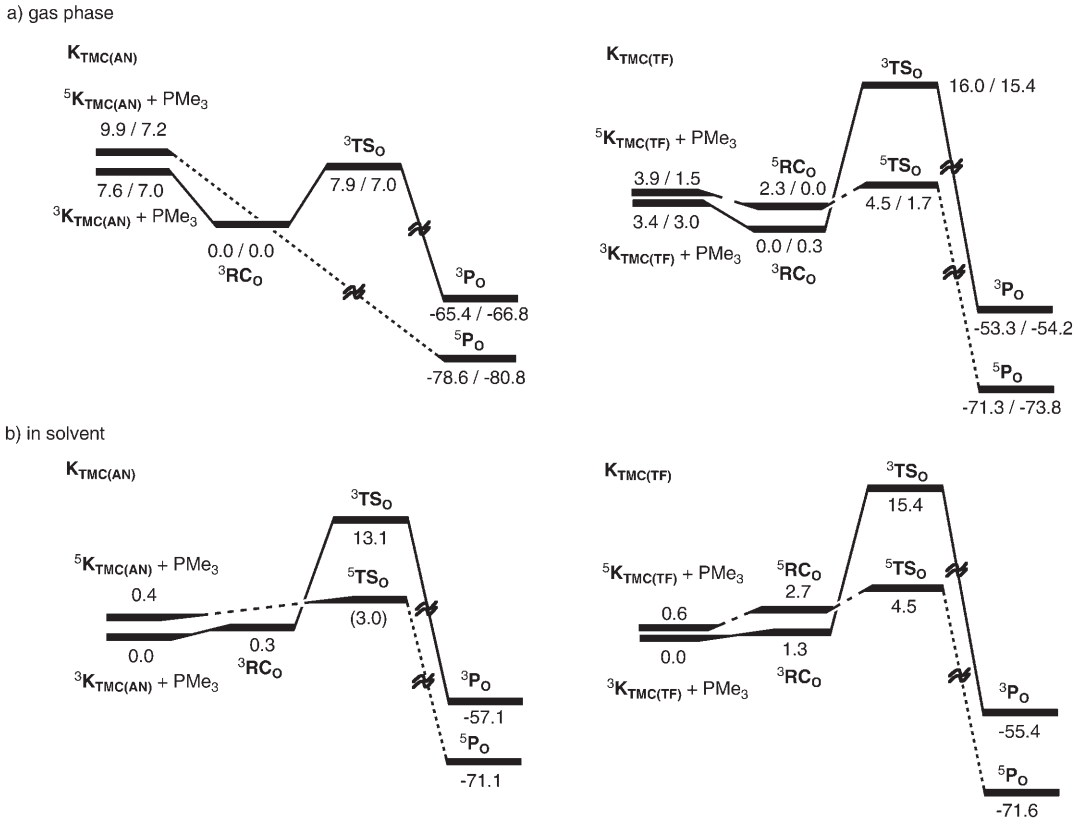

Figure 3. UB3LYP energy profiles for the reaction of $^{3,5}\mathbf{K_{TMC(AN)}}$ and $^{3,5}\mathbf{K_{TMC(TF)}}$ with PMe_3 in the triplet and quintet states: a) The energy profile in the gas phase. Each species has two energy values, corresponding to UB3LYP/B2//B1 and UB3LYP/B2//B1+ZPE, respectively. b) The energy profile in an acetonitrile solution. Here the energy data involve the solvation correction, UB3LYP/B2//B1+ZPE+E_{solv}. The ZPE for $^{5}\mathbf{TS_O}$ for the reaction of $^{5}\mathbf{K_{TMC(AN)}}$ in solution is estimated (see Figure SB17 in the Supporting Information).

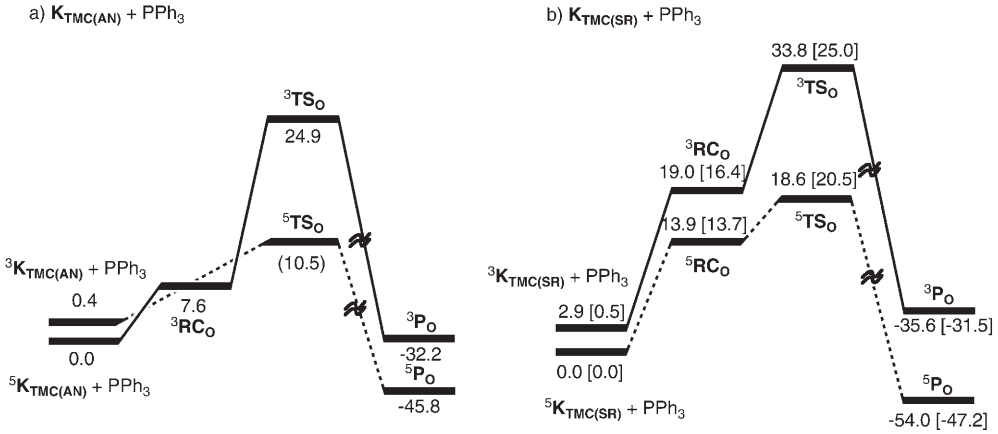

Figure 4. Energy profiles (UB3LYP/B2//B1+ZPE+E_{solv}) for the reactions of $^{3,5}\mathbf{K_{TMC(L)}}$ with PPh_3 for L=AN and SR. The ZPE correction for $^{5}\mathbf{TS_O}$(AN) was estimated (see Figure SB17 in the Supporting Information). In square brackets for L=SR are UB3LYP*/B2//UB3LYP/B1+ZPE+E_{solv} values.

the $^{2S+1}\mathbf{TS_O}$ species gets progressively later, as the electron-releasing power of the ligand increases from L=AN to SR, in accord with the increase in the barriers in the same order. Except for these differences, there are notable similarities for the transition states of two spin states; thus, in both the $^{5}\mathbf{TS_O}$ and $^{3}\mathbf{TS_O}$ structures, the Fe-O-P angles are as large as 160–178°.

Based on the previous analysis of reactivity in nonheme systems,[30] the structures of the transition states reflect the orbital selection rule that governs the bonding in the transition states based on the "oxidation state formalism".[48] Thus, as shown in Scheme 4, in both cases O-transfer occurs in a single step, and hence, the establishment of the transition state is attended by electron shifts from the phosphine

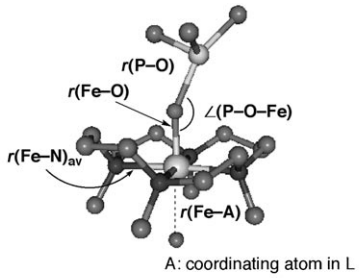

PMe_3 reactions

L	r(P–O)	r(Fe–O)	r(Fe–A)	$r(Fe–N)_{av}$	∠(P–O–Fe)
AN	2.29 [2.95]	1.78 [1.69]	2.23 [2.20]	2.14 [2.24]	157.9 [178.1]
TF	2.14 [2.74]	1.85 [1.71]	2.05 [2.00]	2.14 [2.24]	158.3 [172.1]
N3	2.08 [2.43]	1.88 [1.78]	2.02 [2.00]	2.15 [2.26]	159.9 [170.8]
SR	2.07 [2.22]	1.91 [1.83]	2.41 [2.47]	2.16 [2.26]	159.7 [164.3]
F	1.99 [2.37]	1.91 [1.78]	1.91 [1.91]	2.12 [2.23]	159.7 [170.0]
NCS	2.08 [2.46]	1.88 [1.77]	2.00 [2.02]	2.15 [2.25]	159.1 [171.0]

PPh_3 reactions

L	r(P–O)	r(Fe–O)	r(Fe–A)	$r(Fe–N)_{av}$	∠(P–O–Fe)
AN	2.36 [2.93]	1.80 [1.69]	2.28 [2.18]	2.14 [2.23]	159.9 [177.5]
N3	2.13 [2.25]	1.89 [1.85]	2.03 [2.04]	2.15 [2.26]	158.5 [168.0]
SR	2.17 [2.21]	1.92 [1.85]	2.41 [2.49]	2.16 [2.26]	160.6 [162.6]

Figure 5. UB3LYP/B1 optimized ^{3}**TS$_O$** [^{5}**TS$_O$**] species for the O-transfer reactions (bond lengths in Å and bond angles in degrees). For the reactions of $\mathbf{K_{TMC(AN)}}$ with PMe_3 and PPh_3, the quintet transition state is the ^{5}**TS$_O$** determined in solution.

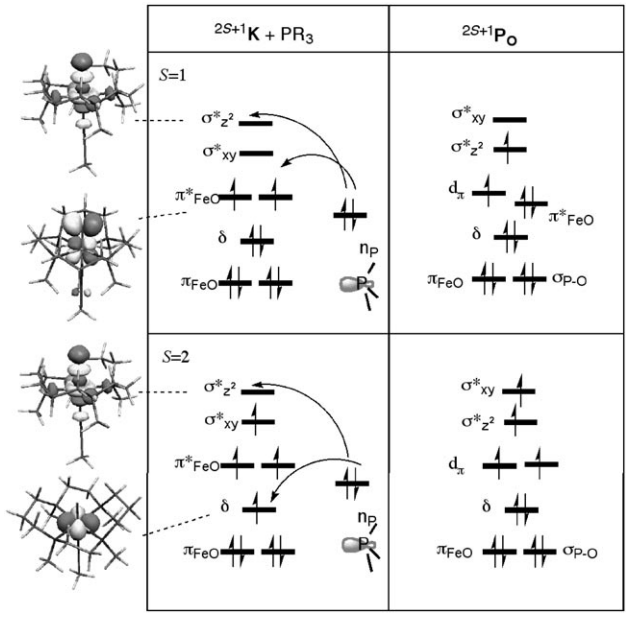

Scheme 4. Electron shifts from the phosphine to the $\mathbf{K_{TMC(L)}}$ during O-transfer.[49]

lone-pair orbital to orbitals of the iron–oxo reagent, and it is the overlap of these orbitals that determines the structure of the transition state. In both the triplet and quintet processes, one electron must be shifted from the phosphine lone-pair to the $\sigma^*_{z^2}$ orbital that lies along the Fe–O axis (see Scheme 4). Therefore, *to maximize the overlap between the phosphorus lone pair and the* $\sigma^*_{z^2}$ *orbital, the* ^{3,5}***TS$_O$*** *species assume structures with large Fe-O-P angles >158°* (see also Figure SB11 in the Supporting Information).[49] Thus, the O-transfer reaction behaves genuinely as a two-electron process, even though the electron-shift events are not strictly synchronous, as may be revealed by the spin density variation in the two processes (see Tables SB1–SB6 and Figure SB12 in the Supporting Information).

H-Abstraction reactions from C_6H_8 by $^{3,5}\mathbf{K_{TMC(L)}}$: Figure 6 shows the energy profiles for H-abstraction by two representative $^{3,5}\mathbf{K_{TMC(L)}}$ complexes, L = AN and TF. The gas-phase energy profiles (Figure 6a) involve reactant clusters, $^{3,5}\mathbf{RC_H}$, followed by transition states for H-abstraction, $^{3,5}\mathbf{TS_H}$, leading to the clusters, $^{3,5}\mathbf{I_H}$, of the radical intermediate $C_6H_7\cdot$ with the iron–hydroxo complexes of $^{3,5}\mathbf{K_{TMC(TF)}}$. However, with $\mathbf{K_{TMC(AN)}}$, the quintet process is calculated to be barrier-free in the gas phase.[30] The high gas-phase electrophilicity of $\mathbf{K_{TMC(AN)}}$ is apparent also from the high positive charge development in the $^3\mathbf{TS_H}$ species (+0.43), and by the fact that as soon as the C_6H_7 moiety was gradually separated from the corresponding iron–hydroxo complex, in $^5\mathbf{I_H}$, it transferred an electron and generated the $C_6H_7^+$ ion.

Aside from this difference, as in the O-transfer reaction, here too there is a TSR scenario nascent from the triplet and quintet states of the reagent. The triplet profiles have significant energy barriers of 11.7 and 19.0 kcal mol^{-1}, via a H-abstraction transition state, $^3\mathbf{TS_H}$. These barriers are reduced to 8.4 and 16.6 kcal mol^{-1} with the inclusion of a ZPE correction; unlike the O-transfer reaction here the ZPE correction is large as would be expected from a C–H activation reaction. The quintet surface is seen to cut through the triplet barrier and, like before,[30] to provide a low-energy path for C–H activation. The barrier for L = TF on the quintet surface is 2.3 kcal mol^{-1} relative to the separate reactants (on the quintet surface). For other ligands, there are even smaller quintet barriers. The energy profile in solution (Figure 6b) shows again that we cannot expect a stable cluster in solution. Otherwise, the main features of the gas-phase profile remain the same in solution; large triplet barriers, 16.4 and 18.5 kcal mol^{-1}, being crossed by the quintet surfaces, which have much smaller barriers (relative to the quintet reactants). The remaining energy profiles have similar characteristics and are collected in the Supporting Information (see Figure SC7 to SC10). As such, all the reactions of the $\mathbf{K_{TMC(L)}}$ reagents proceed by a TSR scenario whereby

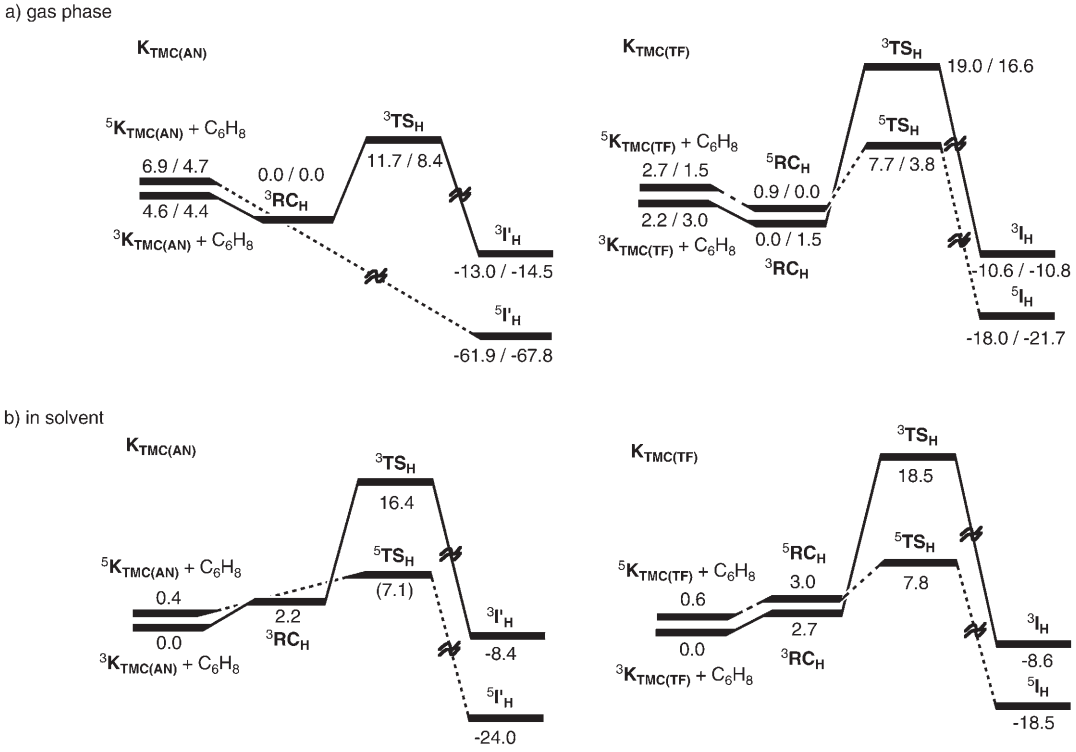

Figure 6. UB3LYP energy profiles for the reaction of $^{3,5}\mathbf{K_{TMC(AN)}}$ and $^{3,5}\mathbf{K_{TMC(TF)}}$ with C_6H_8 in the triplet and quintet states: a) The energy profile in the gas phase. Each species has two energy values, which correspond to UB3LYP/B2//B1 and UB3LYP//B2/B1+ZPE, respectively. b) The energy profile in acetonitrile solution. Here the energy data involve solvation correction, (E(UB3LYP//B2/B1)+ZPE+E_{solv}). The relative energy for $^{5}\mathbf{TS_H}$ in solution for $^{5}\mathbf{K_{TMC(AN)}}$ was obtained by using an estimated ZPE value (see Figure SC13 in the Supporting Information).

the quintet surface cuts through the triplet surface and provides in principle a low-energy path for the transformation. Furthermore, all *the gas-phase barriers on the quintet surface are very small (2–4 kcal mol^{-1}) of the order of the zero-point energy stored in the C–H bond* (ca. 4 kcal mol^{-1}).

The key geometric features of the $\mathbf{TS_H}$ species are given in Figure 7; the structures basically resemble those found in our previous study.[30] Thus, all the structures involve a collinear O–H–C moiety, which is typical of H-abstraction processes. Much in line with the relative barriers on the two spin-state surfaces, the C–H bond lengths in $^{5}\mathbf{TS_H}$ are shorter than in $^{3}\mathbf{TS_H}$, while the H–O bonds are longer. As such, all the $^{5}\mathbf{TS_H}$ species lie earlier on the H-atom transfer coordinate than their corresponding $^{3}\mathbf{TS_H}$ species, a trend which is in accord with the lower barriers and the more exothermic H-atom abstraction energy compared with the triplet process. Another difference between the transition states is apparent in their different Fe-O-H angles, close to 180° for $^{5}\mathbf{TS_H}$ and 143–148° for $^{3}\mathbf{TS_H}$.

The differences in transition-state structures between the two spin states reflect the different selection rules for these transition states, as described in detail in the previous study.[30] As before, this can be understood by reference to the electronic reorganization (following the oxidation state formalism[30,48]), which occurs during the establishment of the transition states. As shown in Scheme 5, during the H-abstraction, there is a shift of an electron from the σ(C–H) bond orbital to the iron–oxo reagent; in the case of $^{5}\mathbf{TS_H}$,

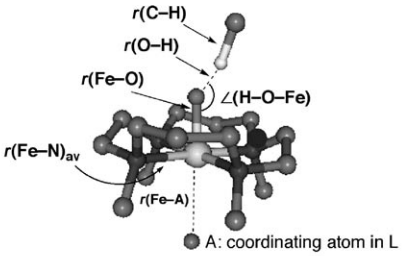

C_6H_8 reactions

L	r(O–H)	r(C–H)	r(Fe–O)	r(Fe–A)	r(Fe–N)$_{av}$	∠(H–O–Fe)
AN	1.41 [1.61]	1.26 [1.16]	1.75 [1.70]	2.13 [2.19]	2.14 [2.24]	147.6 [177.3]
TF	1.32 [1.47]	1.29 [1.20]	1.76 [1.73]	1.99 [2.00]	2.14 [2.24]	146.3 [177.7]
N3	1.33 [1.42]	1.29 [1.22]	1.79 [1.76]	1.97 [1.99]	2.14 [2.25]	143.9 [178.0]
SR	1.31 [1.37]	1.29 [1.25]	1.80 [1.76]	2.36 [2.42]	2.15 [2.25]	147.8 [177.1]
F	1.32 [1.43]	1.30 [1.21]	1.78 [1.74]	1.86 [1.89]	2.11 [2.22]	143.5 [176.3]
NCS	1.33 [1.43]	1.29 [1.22]	1.78 [1.75]	1.94 [1.99]	2.14 [2.25]	144.6 [177.2]

Figure 7. UB3LYP/B1 optimized $^{3}\mathbf{TS_H}$ [$^{5}\mathbf{TS_H}$] species for the H-abstraction reactions (bond lengths in Å and bond angles in degrees). The $^{5}\mathbf{TS}_{H}$ species for L = AN correspond to the solvent-optimized species.

the electron is shifted to $\sigma^*_{z^2}$ orbital that is aligned along the Fe–O axis; this requires a collinear Fe-O-H-C arrangement in the transition state. On the other hand, in the case of ^{3}**TS$_H$** the electron is shifted to the π^*(FeO) orbital, thereby leading to a transition state with a bent Fe-O-H angle. Scheme 5 further shows that the quintet process enjoys a large increase of exchange interactions compared with the triplet species, and hence, as a rule,[30] the quintet barriers are smaller than the corresponding triplet ones. It should also be noted by comparison of Scheme 4 and Scheme 5 that, unlike the O-transfer reaction that behaves as a two-electron process (Scheme 4), *H-abstraction behaves as a one-electron process (still having a redox character due to the change in the oxidation state of iron).*

Table 1. Energy barriers (in kcal mol^{-1}) in the O-transfer reactions of $^{2S+1}$**K$_{TMC(L)}$** with PMe_3 and PPh_3.

L	B1+ZPE	B2+ZPE	B1+ZPE+E_{solv}	B2+ZPE+E_{solv}[a]	$\Delta G^{\neq}$ (B2)[a,b]
a) $S=1$					
AN	7.1	7.0	14.5	13.1 (24.9)	24.3 (41.2)
TF	16.7	15.4	20.3	15.4	27.3
F	19.5	14.9	23.6	18.2	29.9
N3	19.5	18.3	20.3	16.9 (29.8)	29.9 (39.5)
NCS	18.9	18.2	18.6	16.0	28.7
SR	20.2	19.7	21.0	19.9 (33.8)	32.9 (48.8)
b) $S=2$					
AN	0.0	0.0	11.0[c]	3.0[c] (10.5)[c]	13.0[d] (20.5)[d]
TF	5.5	1.7	10.7	4.5	13.9
F	10.7	4.8	15.3	8.8	18.6
N3	6.5	3.9	9.7	4.8 (15.4)	15.9 (25.8)
NCS	7.4	4.5	10.2	5.6	16.2
SR	10.3	7.9	11.2	8.2 (18.6)	21.0 (33.6)

[a] Values in parentheses correspond to the barriers with PPh_3. The datum for the reaction between ^{5}**K$_{TMC(AN)}$** and PPh_3 at $S=2$ is based on the ^{5}**TS$_O$** species obtained at the B1+E_{solv} level discussed above. [b] The free energy barriers are obtained by adding the computed gas-phase thermal and entropic contributions to the B2+ZPE+E_{solv} data. [c] Estimated ZPE values were used. [d] $\Delta_{corr}=10$ kcal mol^{-1} was used for thermal and entropic contribution to the free energy barrier.

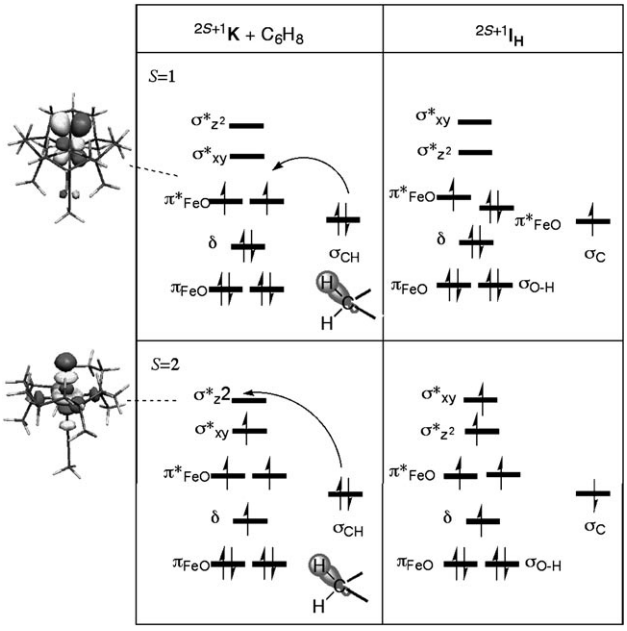

Scheme 5. Electronic reorganization in the H-abstraction process of $^{2S+1}$**K$_{TMC(L)}$**

Discussion of Trends in the O-Transfer and H-Abstraction Barriers of ^{3,5}K$_{TMC(L)}$ Reagents

To facilitate the discussion of the barriers and the reactivity trends, we have collected the computed barriers in Table 1 and Table 2 at various levels. These data and the energy profiles in Figure 3, Figure 4, Figure 5, Figure 7, and Figure 8 will serve as the basis for the discussion.

The following trends are apparent from the data. The first trend, in all the series of the computed barriers, is that on *either the triplet or the quintet surface, the barriers follow the electrophilicity of the $^{2S+1}$**K$_{TMC(L)}$** reagents*; the barriers are low, when L is neutral (AN), and increase when the charge of L is −1. A pictorial representation of this general trend is seen in Figure 8, where *all* the triplet barriers/free energy barriers are drawn against the corresponding $|\Delta q_{CT}|$ quantity (this is the absolute magnitude of charge transferred from the ligand L to the TMC–FeO^{2+} moiety; see Figure 2b). The trends in Figure 8 follow the electrophilicity of the iron–oxo reagent, and are common generally to all the other data sets (including the quintet ones) in Table 1 and Table 2.

It is thus natural to expect that electrophilic reactions, like the ones we calculated in this study, will follow the electrophilicity of the iron–oxo reagent. However experiment disagrees with the computational trends, as illustrated by Figure 9, which plots experimental free-energy barriers derived from the bimolecular rate constant data[26] for the reactions of **K$_{TMC(L)}$** with PPh_3 and DHA (estimation of free energy barriers relied on the Eyring equations; for further details see Figure SA6 in the Supporting Information) versus the electron-releasing index of the ligand, $|\Delta q_{CT}|$ and the calculated triplet–quintet gap (ΔE(Q−T)). *For O-transfer reactivity, theory is in accord with experiment*, with the most electrophilic **K$_{TMC(AN)}$** reacting the fastest with PPh_3 and the least electrophilic **K$_{TMC(SR)}$** reacting the slowest. *For H-abstraction however, the experimental reactivity trend (*Figure 9*) is opposite to that of the computational data* (Figure 8) at all levels and for both spin states.

To ascertain whether or not the experimental H-abstraction trends *may be determined* by the strength of the formed TMC(L)FeO–H bond, we computed the bond dissociation energies (BDEs) of the O–H bond in the TMC(L)FeO–H species for both spin states. The resulting BDEs for the triplet surface (see Table SA5 in the Supporting Information) are fairly constant, and cannot predict the observed trend

Table 2. Energy barriers (in kcal mol^{-1}) in the H-abstraction reactions of $^{2S+1}\mathbf{K}_{\mathbf{TMC(L)}}$ with C_6H_8.

L	B1+ZPE	B2+ZPE	B1+ZPE+E_{solv}	B2+ZPE+E_{solv}	$\Delta G^{\neq}$ (B2)[a]
a) $S=1$					
AN	6.0	8.4	13.9	16.4	29.2
TF	13.2	16.6	15.9	18.5	30.1
F	13.5	16.2	17.4	21.3	32.8
N3	13.7	18.5	16.9	20.1	33.7
NCS	13.8	17.6	15.8	19.5	34.3
SR	14.3	19.7	15.7	21.8	34.3
b) $S=2$					
AN	0.0	0.0	9.5[b]	7.1[b]	17.1[c]
TF	4.0	3.8	7.9	7.8	17.4
F	8.0	5.9	11.9	10.9	20.8
N3	4.0	5.2	7.8	8.5	20.1
NCS	5.3	4.9	9.3	9.7	21.3
SR	5.8	8.2	8.2	11.3	21.6

[a] The free energy barriers are obtained by adding the computed gas-phase thermal and entropic contributions to the B2+ZPE+E_{solv} data. [b] This value is based on the $^5\mathbf{TS_H}$ species located in solution. Estimated ZPE values were used. [c] $\Delta_{corr}=10$ kcal mol^{-1} was used for thermal and entropic contributions to the free energy.

(BDE $\approx$88 kcal mol^{-1} at the B3LYP/B2//B1 level; 90 kcal mol^{-1} for SR and 91 for AN). If we include the interactions in the H-abstraction intermediate, the strongest O–H bond is for L=AN (Method 1 in Table SA5 in the Supporting Information), and the BDE prediction is again in discord with experiment. Using pK_a(TMC(L)FeO–H) as a potential predictor of the trends does not resolve the difficulty either. The pK_a quantity is a combination of the BDE(O–H) and the reduction potential of the iron–oxo species. Since BDE(O–H) is constant, the only variable that determines pK_a is the reduction potential. As we already stated, the experimental measurements[26] show that the relative reactivity behaves opposite to the trend in the reduction peak potentials of the $\mathbf{K}_{\mathbf{TMC(L)}}$ reagents. We may conclude therefore, that the thermodynamics of the H-abstraction process on the triplet surface, or for going from triplet to quintet, appear not to predict correctly

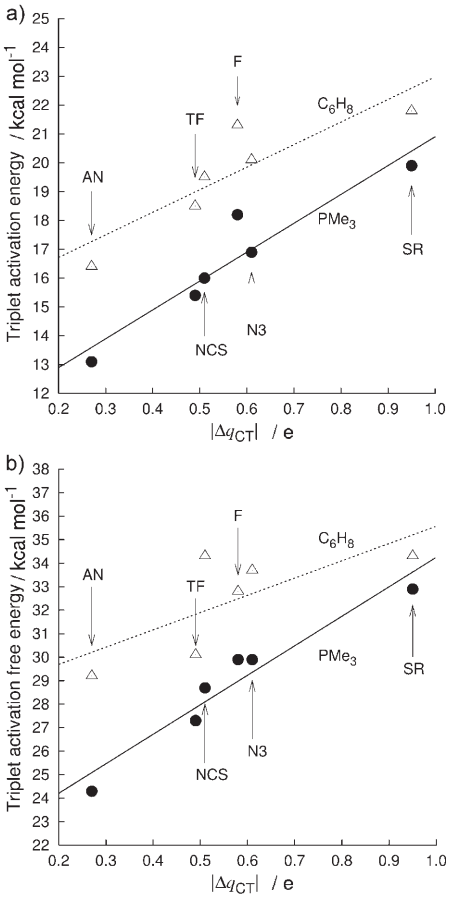

Figure 8. Plots of the calculated barriers at the a) B2//B1+ZPE+E_{solv} level and b) free energy barriers at the B2//B1+ZPE+E_{solv}+Δ_{corr} level for O-transfer (filled circles) and H-abstraction (triangles) reactions versus $|\Delta q_{CT}|$. All barriers are gauged relative to the separate reactants at the lowest state.

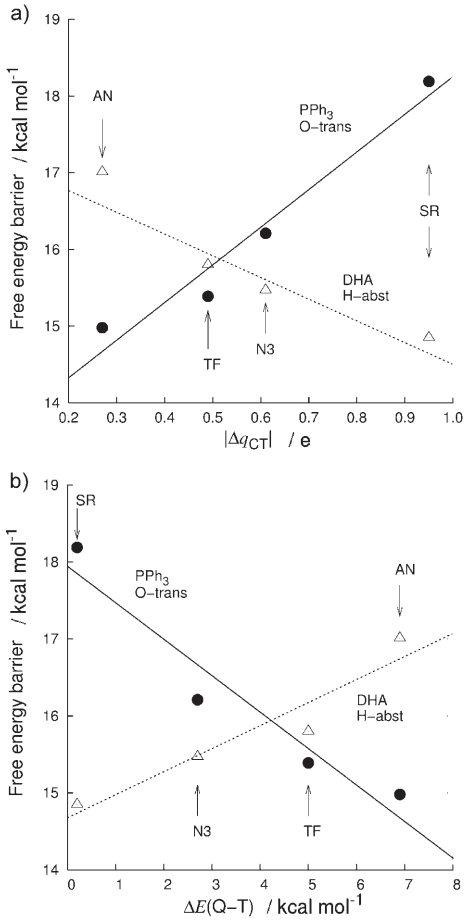

Figure 9. Plots of experimental $\Delta G^{\neq}$ values against a) $|\Delta q_{CT}|$ and b) ΔE-(Q–T). Full circles are O-transfer (P-oxidation) activation data, while triangles are H-abstraction data.

either the computed or the observed trends. On the quintet surface, the largest BDE is for L = AN and the weakest is for L = SR (see Table SA5 in the Supporting Information), and this is in accord with the computed trend in the barriers, but again in discord with experiment. Thus, the computational data show that one cannot invoke a rate-equilibrium relationship that will account for the experimental observations.

From the above discussion it follows that the computed barrier trends constitute a chemically reasonable trend for an oxidative process, such that an electron releasing axial ligand destabilizes the transition state and raises the barrier. The only problem is that the experimental trends for H-abstraction defy this logic (compare Figures 8 and 9). How can we understand the disparity between experimental trends and the theoretical results that are otherwise reasonable and uniform at all levels?

TSR reproduces the trends in the O-transfer and H-abstraction reactions: A potential way to understand these trends may be constructed from the fact that all the energy profiles exhibit two-state reactivity (TSR).[30,50–52] Thus the quintet surface cuts through the triplet barrier, thereby providing in principle a low-energy path for the reactions. But this low energy path requires spin inversion from triplet to quintet, which may serve as an additional bottleneck for the reaction.[30,50,51] We shall therefore consider TSR and examine three different scenarios.

The first scenario that should be examined assumes the existence of *a fast spin pre-equilibrium* between the quintet and triplet $\mathbf{K_{TMC(L)}}$ species, followed by a reaction from the quintet state alone.[30] However, as we saw already in Table 1 and Table 2, while a quintet-state reactivity predicts the trends for the O-transfer to PMe_3, it certainly does not reveal how the counterintuitive reactivity trend in the C–H activation could arise from this scenario. Thus, the hypothesis of fast spin pre-equilibrium and a follow-up reaction from the quintet spin-state surface has to be ruled out *because the trends in C–H reactivity on any one of the spin surfaces follow electrophilicity.* In addition, experimental data[26–28] show no apparent signs for spin pre-equilibrium and all the complexes have spectral properties of ground state triplet species.

Another TSR scenario is one in which the reaction starts on the triplet-state surface and, *en route* to the **TS**, crosses over to the quintet surface with a probability that depends, inter alia, on the spin-orbit coupling (SOC) interaction between the two spin states.[50–52] This SOC matrix element[50] is a monoelectronic matrix element between two orbitals: one is the orbital that is depopulated in the crossover of the triplet to quintet, and the other is the orbital that is populated in the same transition. At the stage of the $\mathbf{K_{TMC(L)}}$ complexes these orbitals are δ and σ^*_{xy} (e.g., Schemes 3 and 5). It is known that the SOC interaction is very sensitive to orbital delocalization and to changes in electronic structure.[50] Thus, SOC is at maximum when the two orbitals are strictly localized on the iron and when the two states have electronic structures that differ by the occupancy of a single d orbital.[30,50] In a former MCSCF study of SOC in the H-abstraction process in the reaction of FeO^+ with H_2, *the SOC interaction was found to vary drastically along the reaction coordinate due to delocalization of the orbitals and to shrink down to zero at the exit channel (Fe^+/H_2O) due to changes in the electronic structure*.[50] For the present system, at the reactant stage, where orbital delocalization is modest, and when the two states differ by a single orbital occupancy[30] the expected SOC matrix element would be significant. However, during H-abstraction, the orbitals of the two states become more delocalized and involve the substrate orbitals, for example, the C–H moiety of the reagent. Furthermore, as can be seen from Scheme 5, during H-abstraction the electronic structure changes and other orbitals become involved too in each one of the states, which now *differ by more than one orbital occupation*. This further reduces the SOC value.[30,50] The larger the initial spin-states energy gap the "later" is the crossing, the more mixed are the orbitals and the more different are the electronic structures of the two states, so that the SOC is expected to become smaller and smaller as the initial energy gap between the state becomes larger.[50] Since the probability of spin crossover is exponential in SOC (e.g., in the Landau–Zener model[50]), we may reason that the probability of triplet-to-quintet crossover should decrease quite fast as the initial quintet-triplet energy gap increases. Following the data in Figure 2, we can expect that *the spin-inversion probability should be smallest for L = AN, with the largest gap, and should increase as the electron releasing power of the axial ligand increases up to L = SR*. The so predicted large SOC mixing for L = SR is in fact supported by analysis of the experimental Mössbauer data,[28] which show that in this complex the quintet state is more extensively mixed into the triplet ground state than in other complexes of this type.

Since in practice there is currently no good way to compute what is needed to model such TSR scenarios, where the reactions take place in solution and where there are so many of them, we must construct these scenarios using a working hypothesis that will serve to reason the reactivity patterns observed experimentally. If successful, such an idea can provide the conceptual means to design reactions that can test the hypothesis and gain thereby improved insight into TSR.

Inspection of the data for C–H activation in Table 2 reveals that one can obtain a counterintuitive reactivity pattern in a TSR scenario where the two states contribute to product formation. Thus, we consider a TSR scenario where most of the process occurs on the quintet surface that has the smaller barriers. However, because the spin inversion probability is low, *there is a high probability of staying on the triplet state*, which may contribute to the overall reactivity (only, of course, if the barrier difference is matched by a low spin inversion probability). Such a scenario can be mimicked by blending the quintet barriers with weighted contributions from the triplet barriers, such that the contribution of the triplet increases as the quintet–triplet energy gap in-

creases.[52] Accordingly, consider the simple expression of the barrier of the reaction as a blend, or a weighted average of the two barriers in Equation (1):

$$\Delta E^{\ddagger}_{QT} = x\Delta E^{\ddagger}_{T} + (1-x)\Delta E^{\ddagger}_{Q} \quad (1)$$

where $\Delta E^{\ddagger}_{QT}$ is the net reaction barrier due to blending of the triplet and quintet barriers, x is the weight of the triplet process in the overall process, and $1-x$ is the quintet weight. In turn, using these barriers in an Arrhenius equation or in the Eyring equation, the corresponding rate constant would be given by Equation (2):

$$k_{TQ} = k^{x}_{T} \cdot k^{(1-x)}_{Q} \quad (2)$$

Thus, the rate constant is a weighted geometric average of the corresponding triplet and quintet rate constants.

Rearrangement of the terms in Equation (1) shows how the blending affects the net barrier [Eq. (3)]:

$$\Delta E^{\ddagger}_{QT} - \Delta E^{\ddagger}_{Q} = x(\Delta\, E^{\ddagger}_{T} - \Delta\, E^{\ddagger}_{Q}) \quad (3)$$

It is seen that relative to the quintet barrier, the net barrier ($\Delta E^{\ddagger}_{QT}$) is raised by a product of the weight of the triplet reaction (x) and the difference between the barriers on the triplet and quintet surfaces, ($\Delta E^{\ddagger}_{T} - \Delta E^{\ddagger}_{Q}$). As such, it is apparent that, as x increases with the quintet–triplet energy gap as would be required by the above reasoned lowering of spin inversion probability (from L = SR to L = AN), so does the barrier. Consequently the relative reactivity in a series can be inverted, from one controlled by the electrophilicity of the reagent (i.e., L = AN is the most reactive) to one that follows the electron-donating power of L (L = SR is the most reactive).

A set of x values can be determined from the computational data by seeking the critical x_c that equalizes the barriers for L = AN and all the other L ligands (see pages S24–S26 in the Supporting Information for details) for both C–H activation and O-transfer series, based on the quintet and triplet barriers in Table 1 and Table 2. Any set of x values larger than the so-determined critical ones will reproduce the counterintuitive trend in the C–H activation barriers, whereas a smaller value will reproduce the trends observed in the O-transfer barriers. Thus, using the free energy barriers in Table 1 and Table 2 (UB3LYP/B2//B1 + ZPE + E_{solv}), the so determined final x values are the following: for the C–H activation series, they are AN ($x = 0.56$), TF ($x = 0.50$), F ($x = 0.10$), N3 ($x = 0.17$), NCS ($x = 0.03$), and SR ($x = 0.00$), while for O-transfer these values are: AN ($x = 0.88$), TF ($x = 0.71$), F ($x = 0.63$), N3 ($x = 0.61$), NCS ($x = 0.67$), and SR ($x = 0.50$). Other sets of the barriers give different values, but what matters more is the trend in the x values, which are determined with no bias; this is seen to increase in the order AN > TF > N3 > SR *exactly as the expected participation of the triplet based on the quintet–triplet energy gap and its effect on lowering of the SOC*; the $\mathbf{K_{TMC(SR)}}$ with the smallest energy gap has the largest participation of the quintet state, whereas $\mathbf{K_{TMC(AN)}}$ with the largest spin-state gap has the smallest quintet participation. The working hypothesis exhibits at least a physically reasonable trend.

Figure 10 shows the so-determined blended computational barriers plotted as a function of $|\Delta q_{CT}|$ in Figure 10a and as a function of the triplet-quintet gap ΔE(Q–T) in Figure 10b. It is seen that the TSR-based blended free energy barriers reproduce the trends observed in the experimental studies. Thus, *the H-abstraction barriers follow the counterintuitive trend* whereby the barriers generally decrease as the electron-releasing power of the ligand L increases and the triplet–quintet energy gap, ΔE(Q–T), decreases. By contrast, the TSR-based blended barriers for the O-transfer series exhibit the opposite trend; the barrier is lowest for L = AN and generally increases with the electron releasing power of L, thus following the electrophilicity of $\mathbf{K_{TMC(L)}}$. In addition, these two sets of TSR-based barriers exhibit reactivity crossover in the series, such that for L = AN the two-electron reactivity in O-transfer is higher than the one-electron reactivity in H-abstraction, and as the ligand becomes

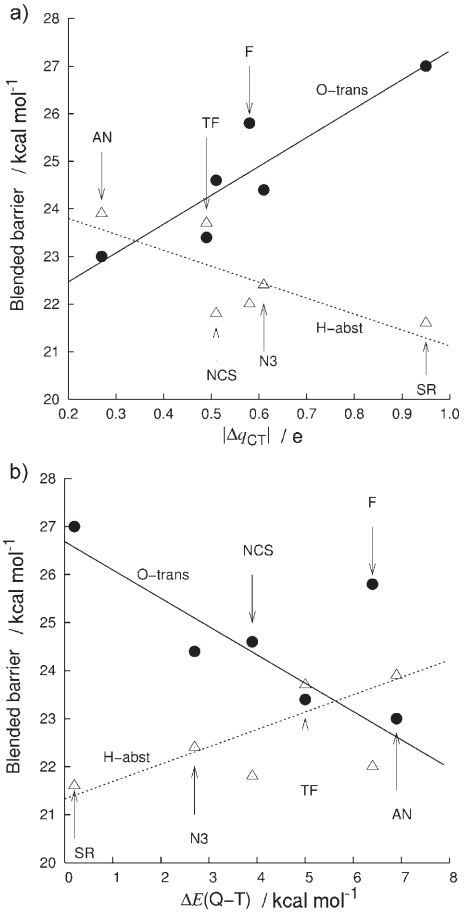

Figure 10. Plots of theoretical TSR-free energy barriers versus the two organizing quantities of the axial ligand effect: a) The behavior of the TSR blended triplet–quintet barriers, determined according to Equation (1), as a function of $|\Delta q_{CT}|$. b) A plot of the same blended triplet–quintet barriers against ΔE(Q–T). Triangles and the dashed line correspond to H-abstraction data, while full circles and the solid line corresponding to P-oxidation data.

more electron rich, the barrier difference decreases and eventually at L=NCS the H-abstraction reactivity becomes dominant. In fact, by removing the points for L=F and NCS for which there are no experimental rate constant data reported, Figure 10 would look much like Figure 9 that exhibits the corresponding experimental data. It further looks like a twin of the plot of the experimental barriers for DHA and PPh_3 found in our previous paper.[26]

After demonstrating the plausibility of the blended-TSR idea by modeling the CHD and PMe_3 data in Figure 10, we can consider the PPh_3 data vis-à-vis the CHD data. From Table 1 it is apparent that the free energy barriers to O-transfer to PPh_3 on the quintet surface follow the electrophilicity of the reagent too. Thus, using the blended C–H activation barriers in Figure 10, and the quintet barriers ($x=0$ for all L values) to O-transfer to PPh_3 will exhibit precisely the same pattern as the one simulated for CHD and PMe_3 in Figure 10. It appears therefore, that the observation of reactivity crossovers in C–H activation of CHD versus O-transfer to PPh_3,[26–28] may correspond to a scenario whereby C–H activation occurs by a blended triplet–quintet reactivity, while the O-transfer reactivity of PPh_3 occurs predominantly on the quintet surface.

An alternative way of blending the two processes was presented in our previous publication,[30] and is given in Equation (4):

$$k_{TQ} = xk_Q + (1-x)k_T \quad (4)$$

Here, the blended rate constant is given as a weighted sum of the states′ rate constant weighted by their corresponding probabilities. In our data, the rate constants on the two states are widely different, so that the triplet rate will not make any substantial contribution to the blend, and will be left with Equation (5), where the rate is given by the rate constant of the quintet surface multiplied by the probability x of crossover from the triplet ground state to the quintet state along the reaction path:

$$k_{TQ} \sim xk_Q \quad (5)$$

This expression is analogous to the traditional TSR model as expressed in Equation (6):[50,51c]

$$k_{TSR} = \kappa_{TQ}k_Q = \kappa_{TQ}(k_BT/h)\exp(-\Delta G_Q^{\ddagger}/RT) \quad (6)$$

This is the usual Eyring equation corrected by a "transmission coefficient" (κ_{TQ}), which depends on the probability of spin crossover from triplet to quintet. Thus, the free energy barriers for this TSR scenario are those on the quintet surface, but the rate is weighted by the probability of crossing over from the triplet ground state to the quintet excited state *en-route* to C–H activation or P-oxidation. As we reasoned above, the SOC interaction, and hence also the spin inversion probability, should be highest for L=SR and lowest for L=AN, and the change is expected to be significant due to orbital delocalization and changes in the electronic structure. Furthermore, since κ_{TQ} varies exponentially with the SOC matrix element squared,[50] which decreases as the triplet–quintet gap increases, it is anticipated that κ_{TQ} will be reduced fairly steeply along the series. Therefore, if we use the quintet free energy barriers for H-abstraction in Table 2, and scale the Eyring rate constant by a spin inversion coefficient (κ_{TQ}) that decreases gradually from L=SR to L=AN, the relative rates in the series will be inverted to yield the observed anti-electrophilic trend.[26] At room temperature, each order of magnitude in rate constant corresponds to 1.4 kcal mol^{-1}, and thus inspection of the quintet free energy barriers (Table 1, data for $S=2$) show that the transmission coefficient will have to decrease by slightly over four orders of magnitude to achieve the counterintuitive reactivity trend (see Supporting Information, p S26). Such a decrease is physically feasible considering the exponential dependence of κ_{TQ} on the SOC matrix element, and the expected decrease of the latter quantity.[50] In the traditional-TSR model too, one can get different values of κ_{TQ} using different barriers sets (e.g., see Supporting Information, p S26), but what matters is that all these numbers exhibit the same physically reasonable trend, namely κ_{TQ} decreases as the initial quintet–triplet energy gap increases, from L=SR to AN.

The two TSR scenarios [Eq. (1) versus Eq. (6)] make equivalent predictions, regarding the above dichotomic reactivity, and the decision between them has to be based on two criteria: i) Which one is more realistic? ii) Which one makes more useful and testable predictions?

One concern regarding the blended-TSR notion is that the quintet barrier is much lower than the triplet barrier (Table 2). So, based on energetic considerations alone, one would not expect a contribution of the triplet reaction (even if the staying probability on the triplet is high), and one should favor the traditional-TSR scenario in Equation (6). However the argument behind this concern does not take into account the fact that the quintet energies are overstabilized in B3LYP (and apparently also in PBE0). In fact, fitting the Mössbauer parameters to experiment for $^3\mathbf{K}_{\mathbf{TMC(SR)}}$ required an upward shift of the computed quintet energy, relative to the triplet state.[28] Such a upward shift in the quintet barriers, along with small spin inversion probabilities (that decrease from L=SR to AN), will render the blended-TSR scenario more plausible. Let us then consider in the next section the predictive insights that can differentiate the two models.

Some predictions of the two-state reactivity approaches: An obvious direction for testing the TSR model is the design of metal–oxo oxidants where the quintet states are high energy and inaccessible. Such complexes, which prefer the lower spin states should be abound by changing the metal, or by proper design of the ligands.[53] For such complexes, the two TSR scenarios predict that: i) both C–H activation and P-oxidation will be sluggish since they cannot enjoy the low energy pathway provided by the quintet state; and that ii) both C–H and P-oxidation will exhibit a reactivity trend in

accord with the relative electrophilicity of the reagents. Another prediction of the two models is the temperature dependence of the rate constant.[50,51c] This is more apparent in Equations (5) and (6), where the spin inversion probability reduces the pre-exponential factor, and would therefore yield highly negative entropy of activation if analyzed by means of the Eyring equation. Thus the TSR models predict that the reaction for L = AN will have the most negative entropy of activation, while L = SR the least negative.

A second approach is to devise experiments that can distinguish between the two TSR models. Two tests come to mind:

The first test is based on the previous computational study of $(N4Py)FeO^{2+}$ and $(Bn\text{-}tpen)FeO^{2+}$,[30] which showed that, after the H-abstraction step, *only the triplet surface encountered a rebound barrier to form an alcohol complex, whereas on the quintet surface there is a barrier-free rebound* (this however, is not the case for $TMC(SR)FeO^{+}$ where a rebound barrier seems to exist[31]). In the traditional-TSR model [Eq. (6)], since all reactivity is channeled via the quintet surface, one would not expect much if any stereochemical scrambling, at least based on the computed energy surfaces for the rebound process of $(N4Py)FeO^{2+}$ and $(Bn\text{-}tpen)FeO^{2+}$.[30] In contrast, in the blended-TSR model, since part of the reaction proceeds on the triplet state, significant scrambling of stereoselectivity is expected. Significant scrambling will thus indicate a blended-TSR reactivity. In such an event, one could use an R–H substrate with a stereochemical label, as, for example, in Scheme 6,

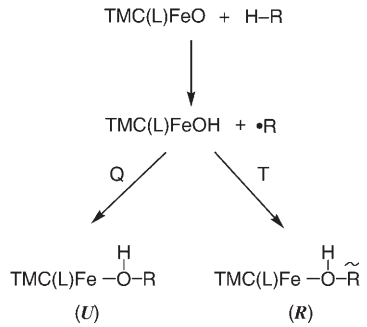

Scheme 6. Rearranged (***R***) and unrearranged (***U***) alcohol products expected from a blended-TSR approach ([Eq. (1)]). The tilde over the R moiety in ***R*** denotes a rearranged organic radical compared with the same moiety in ***U***.

and analyze the alcohol product. As shown in Scheme 6, the value of x ([Eq. (1)]) can be determined from the ratio of the rearranged alcohol (***R***) yield, to the total alcohol yield, involving the sum of unrearranged (***U***) and rearranged alcohol (***R***) product yields.

The second test is based on kinetic isotope effect (KIE) measurements. In the blended-TSR approach ([Eqs. (1) and (4)]) the KIE will have two contributions, one coming from the quintet surface, the other from the triplet. Using equation 2, the KIE in blended-TSR can be broken down into the individual contributions as in Equation (7):

$$KIE_{TQ} = KIE_T^x \cdot KIE_Q^{(1-x)} \quad (7)$$

Since the quintet *gas-phase barrier* for C–H abstraction from C_6H_8 is extremely small, 2–4 kcal mol^{-1}, one can imagine that once there is a spin crossover from the triplet to the quintet surface, *the zero-point energy stored in the C–H bond ($\approx$4 kcal mol^{-1}) is sufficient to propagate the molecular system across the quintet barrier, within a single vibrational amplitude (the ZPE of the C–D bond will not be sufficient and the reaction will proceed by normal activation over a barrier)*. Such a mechanism will give rise to a very large KIE much like a tunneling process.[54] Thus, we may conclude that the KIE_Q value should be very large for most cases with weak C–H bonds like C_6H_8. In contrast, with strong C–H bonds, generally, the quintet energy barrier will be often larger than the ZPE of the C–H bond and the quintet-state bond activation will proceed in a normal activation over the barrier, giving rise to semiclassical KIE (7 or so).

From the work on the TauD enzyme,[8] an iron–oxo active species *with a quintet ground state* exhibits a KIE > 30, much larger than the computed semiclassical value. Indeed the semiclassical values calculated by us for $\mathbf{K_{TMC(L)}}$ in the quintet state are very small, 3.7–6.1 (see Table SC11 in the Supporting Information) in accord with the small value reported by de Visser for the TauD model reaction.[55] Therefore, assuming that the KIE_T value is semiclassical, (KIE_T = 5.8–7.0; see Table SC11 in the Supporting Information), as observed in similar H-abstraction processes,[2] one can predict that within a series of the type used here, the blended-TSR based KIE_{TQ} will be smallest for L = AN and largest for L = SR. *Qualitative support for this prediction can be found in the experimental data for the* Fe(O)(TMC)(L) *complexes discussed in this paper where observed KIE values range from 10–20 for the activation of weak C–H bonds.*[26] Generally, in a series where an iron–oxo reagent reacts with alkanes with different C–H bond strengths, one would expect a highly variable KIE, stretching from semiclassical to nonclassical values, depending on the C–H bond strength and reflecting the blending of the triplet into the quintet processes. Indeed, experimental KIE values have been observed to range from 10 to 60.[16,19,20,26]

Although such observations do not rule out the traditional-TSR scenario ([Eq. (6)]), it is less clear at the moment how it could account for or predict such high variability of the KIE. The blended TSR in Equation (4) does not give a clear breakdown of the KIE_{TQ} into individual components, but it is expected to yield similar predictions to Equation (2).

Concluding Remarks

The hydrogen abstraction (H-abstraction) and phosphine oxidation (P-oxidation) reactions of nonheme Fe^{IV}=O reagents exhibit two-state reactivity (TSR), in which the ground triplet state possesses large barriers for bond activa-

tion, whereas the thermally accessible quintet state has smaller barriers that provide the system with a low energy path for bond activation. Scheme 4 and Scheme 5 delineate orbital selection rules that underlie the different reactivity features of the two spin-state surfaces. The schemes project also that the physical basis for the small quintet-state barriers is the increase of the number of exchange interactions in the quintet transition state. This reasoning makes TSR a plausible reactivity scenario for bond activation by nonheme Fe^{IV}=O complexes.

Equations (1)–(6) constitute two schemes for analysis of TSR situations that are similar to the ones studied here, wherein the reactivity reflects the influence of the two spin states, either via the transmission coefficient [Eq. (6)] or via the blend of the barriers of the individual states [eqs. (1)–(5)] that contribute to the overall process. In either formulation one can rationalize the counterintuitive reactivity observed in H-abstraction,[26] and the reactivity crossover of the H-abstraction and P-oxidation series.[26–28]

From the analysis of the blended-TSR barriers, it is apparent that the experimental observation may not constitute a generally expected phenomenon that should characterize any series of C–H activation versus O-transfer reactions with a given set of iron–oxo reagents. The so-obtained enigmatic results correspond to the specific series used in the experimental study, and could be modeled here with TSR [Eqs. (1)–(6)]. Nevertheless, the basic equations of blended-TSR, Equations (1) and (3), also predict that as the C–H bond strength in the substrate increases, the quintet barrier will increase, and the relative reactivity of the $\mathbf{K_{TMC(L)}}$ series will be less responsive to the electron-releasing power of L but will follow the electrophilicity of the iron–oxo reagent. The fundamental message is that the occurrence of both the counterintuitive trend (for C–H activation) as well as the more intuitive reactivity pattern (for O-transfer) results from the TSR scenario where two spin states interplay and give rise to the overall reactivity. The blended-TSR scenario makes additional testable predictions on radical clock substrates, on KIE patterns, as well as on complexes with inaccessible quintet states that cannot exhibit TSR.

One would have certainly liked to have more precise computational techniques that would have allowed an assessment of the various TSR approaches more quantitatively. However, at present this is not realistic. The above testable predictions constitute at present more realistic probes that will determine eventually the status of this model.

Acknowledgements

H.H. was supported by JSPS Postdoctoral Fellowships for Research Abroad. S.S. acknowledges support by the German Federal Ministry of Education and Research within the framework of the German–Israeli Project Cooperation (DIP). L.Q. is grateful for the support by the NIH (GM-33162). W.N. is grateful for financial support from KOSEF/MOST through Creative Research Initiative Program.

[1] M. Sono, M. P. Roach, E. D. Coulter, J. H. Dawson, *Chem. Rev.* **1996**, *96*, 2841–2888.
[2] J. T. Groves in *Cytochrome P450: Structure, Mechanism, and Biochemistry*, 3rd ed. (Ed.: P. R. Ortiz de Montellano), Kluwer-Academic/Plenum, New York, **2005**, pp 1–43.
[3] I. Schlichting, J. Berendzen, K. Chu, A. M. Stock, S. A. Maves, D. E. Benson, R. M. Sweet, D. Ringe, G. A. Petsko, S. G. Sligar, *Science* **2000**, *287*, 1615–1622.
[4] T. Spolitak, J. H. Dawson, D. P. Ballou, *J. Biol. Chem.* **2005**, *280*, 20300–20309.
[5] I. G. Denisov, T. M. Makris, S. G. Sligar, *J. Biol. Chem.* **2001**, *276*, 11648–11652.
[6] T. S. Dowers, D. A. Rock, D. A. Rock, J. P. Jones, *J. Am. Chem. Soc.* **2004**, *126*, 8868–8869.
[7] D. L. Harris, *Curr. Opin. Chem. Biol.* **2001**, *5*, 724–735.
[8] J. C. Price, E. W. Barr, T. E. Glass, C. Krebs, J. M. Bollinger, Jr., *J. Am. Chem. Soc.* **2003**, *125*, 13008–13009.
[9] J. C. Price, E. W. Barr, B. Tirupati, J. M. Bollinger, Jr., C. Krebs, *Biochemistry* **2003**, *42*, 7497–7508.
[10] D. A. Proshlyakov, T. F. Henshaw, G. R. Monterosso, M. J. Ryle, R. P. Hausinger, *J. Am. Chem. Soc.* **2004**, *126*, 1022–1023.
[11] L. M. Hoffart, E. W. Barr, R. B. Guyer, J. M. Bollinger, Jr., C. Krebs, *Proc. Natl. Acad. Sci. USA* **2006**, *103*, 14738–14743.
[12] D. P. Galonic, E. W. Barr, C. T. Walsh, J. M. Bollinger, Jr., C. Krebs, *Nat. Chem. Biol.* **2007**, *3*, 113–116.
[13] J.-U. Rohde, J.-H. In, M. H. Lim, W. W. Brennessel, M. R. Bukowski, A. Stubna, E. Münck, W. Nam, L. Que, Jr., *Science* **2003**, *299*, 1037–1039.
[14] a) M. Costas, M. P. Mehn, M. P. Jensen, L. Que, Jr., *Chem. Rev.* **2004**, *104*, 939–986; b) W. Nam, *Acc. Chem. Res.* **2007**, *40*, 522–531.
[15] X. Shan, L. Que, Jr. *J. Inorg. Biochem.* **2006**, *100*, 421–433.
[16] J. Kaizer, E. J. Klinker, N. Y. Oh, J.-U. Rohde, W. J. Song, A. Stubna, J. Kim, E. Münck, W. Nam, L. Que, Jr. *J. Am. Chem. Soc.* **2004**, *126*, 472–473.
[17] V. Balland, M.-F. Charlot, F. Banse, J.-J. Girerd, T. A. Mattioli, E. Bill, J.-F. Bartoli, P. Battioni, D. Mansuy, *Eur. J. Inorg. Chem.* **2004**, *2*, 301–308.
[18] M. Martinho, F. Banse, J.-F. Bartoli, T. A. Mattioli, P. Battioni, O. Horner, S. Bourcier, J.-J. Girerd, *Inorg. Chem.* **2005**, *44*, 9592–9596.
[19] N. Y. Oh, Y. Suh, M. J. Park, M. S. Seo, J. Kim, W. Nam, *Angew. Chem.* **2005**, *117*, 4307–4311; *Angew. Chem. Int. Ed.* **2005**, *44*, 4235–4239.
[20] T. K. Paine, M. Costas, J. Kaizer, L. Que, Jr., *J. Biol. Inorg. Chem.* **2006**, *11*, 272–276.
[21] M. H. Lim, J.-U. Rohde, A. Stubna, M. R. Bukowski, M. Costas, R. Y. N. Ho, E. Münck, W. Nam, L. Que, Jr., *Proc. Natl. Acad. Sci. USA* **2003**, *100*, 3665–3670.
[22] S. O. Kim, C. V. Sastri, M. S. Seo, J. Kim, W. Nam, *J. Am. Chem. Soc.* **2005**, *127*, 4178–4179.
[23] C. V. Sastri, M. J. Park, T. Ohta, T. A. Jackson, A. Stubna, M. S. Seo, J. Lee, J. Kim, T. Kitagawa, E. Munck, L. Que, Jr., W. Nam, *J. Am. Chem. Soc.* **2005**, *127*, 12494–12495.
[24] C. V. Sastri, M. S. Seo, M. J. Park, K. M. Kim, W. Nam, *Chem. Commun.* **2005**, 1405–1407.
[25] M. You, M. S. Seo, K. M. Kim, W. Nam, J. Kim, *Bull. Korean Chem. Soc.* **2006**, *27*, 1140–1144.
[26] C. V. Sastri, J. Lee, K. Oh, Y. J. Lee, J. Lee, T. A. Jackson, K. Ray, H. Hirao, W. Shin, J. A. Halfen, J. Kim, L. Que, Jr., S. Shaik, W. Nam, *Proc. Natl. Acad. Sci. USA*, **2007**, *104*, 19181–19186.
[27] J.-U. Rohde, L. Que, Jr., *Angew. Chem.* **2005**, *117*, 2295–2298; *Angew. Chem. Int. Ed.* **2005**, *44*, 2255–2258.
[28] M. R. Bukowski, K. D. Koehntop, A. Stubna, E. L. Bominaar, J. A. Halfen, E. Münck, W. Nam, L. Que, Jr., *Science* **2005**, *310*, 1000–1002.
[29] A. Decker, E. I. Solomon, *Angew. Chem.* **2005**, *117*, 2292–2295; *Angew. Chem. Int. Ed.* **2005**, *44*, 2252–2255.
[30] H. Hirao, D. Kumar, L. Que, Jr., S. Shaik, *J. Am. Chem. Soc.* **2006**, *128*, 8590–8606.

[31] S. P. de Visser, *J. Am. Chem. Soc.* **2006**, *128*, 15809–15818.
[32] Jaguar 5.5, Schrödinger, Inc., Portland, Oregon, **2004**.
[33] M. J. Frisch, et al. Gaussian 03, Revision C.02. Gaussian, Inc., Wallingford CT, **2004**.
[34] a) A. D. Becke, *J. Chem. Phys.* **1992**, *96*, 2155–2160; b) A. D. Becke, *J. Chem. Phys.* **1992**, *97*, 9173–9177; c) A. D. Becke, *J. Chem. Phys.* **1993**, *98*, 5648–5652; d) C. Lee, W. Yang, R. G. Parr, *Phys. Rev. B* **1988**, *37*,785–789.
[35] The LACVP series is derived from LANL2DZ, see: a) J. P. Hay, W. R. Wadt, *J. Chem. Phys.* **1985**, *82*, 299–310; b) R. A. Friesner, R. B. Murphy, M. D. Beachy, M. N. Ringnalda, W. T. Pollard, B. D. Dunietz, Y. Cao, *J. Phys. Chem. A* **1999**, *103*, 1913–1928.
[36] H. Hirao, D. Kumar, S. Shaik, *J. Inorg. Biochem.* **2006**, *100*, 2054–2068.
[37] a) P. Flükiger, H. P. Lüthi, S. Portmann, J. Weber, Mokelel 4.3 and 5.1.0, Swiss Center for Scientific Computing, Manno, Switzerland, **2000–2002**; b) S. Portmann, H. P. Lüthi, *CHIMIA* **2000**, *54*, 766–770.
[38] C. Adamo, V. Barone, *J. Chem. Phys.* **1999**, *110*, 6158–6170.
[39] a) A. Fouqueau, M. E. Casida, L. M. Lawson Daku, A. Houser, F. Neese, *J. Chem. Phys.* **2005**, *122*, 044110/1–044110/13; b) F. Neese, *J. Inorg. Biochem.* **2006**, *100*, 716–726; c) J. C. Schnöboom, F. Neese, W. Thiel, *J. Am. Chem. Soc.* **2005**, *127*, 5840–5853.
[40] M. Reiher, O. Salomon, B. A. Hess, *Theor. Chem. Acc.* **2001**, *107*, 48–55.
[41] a) M. Dolg, U. Wedig, H. Stoll, H. Preuss, *J. Chem. Phys.* **1987**, *86*, 866–872; b) A. J. H. Wachters, *J. Chem. Phys.* **1970**, *52*, 1033–1036; c) C. W. Bauschlicher, Jr., S. R. Langhoff, L. A. Barnes, *J. Chem. Phys.* **1989**, *91*, 2399–2411.
[42] B. J. Lynch, Y. Zhao, D. G. Truhlar, *J. Phys. Chem. A* **2003**, *107*, 1384–1388.
[43] D. J. Tannor, B. Marten, R. Murphy, R. A. Friesner, D. Sitkoff, A. Nicholls, M. Ringnalda, W. A. Goddard, III, B. Honig, *J. Am. Chem. Soc.* **1994**, *116*, 11875–11882.
[44] S. P. de Visser, F. Ogliaro, P. K. Sharma, S. Shaik, *J. Am. Chem. Soc.* **2002**, *124*, 11809–11826.
[45] L. Melander, W. H. Saunders, Jr., *Reaction Rates of Isotopic Molecules*, Robert E. Krieger Publishing Company, Malabar, Florida, **1987**.
[46] H. Hirao, D. Kumar, W. Thiel, S. Shaik, *J. Am. Chem. Soc.* **2005**, *127*, 13007–13018.
[47] D. Kumar, H. Hirao, L. Que, Jr., S. Shaik, *J. Am. Chem. Soc.* **2005**, *127*, 8026–8027.
[48] S. Shaik, D. Kumar, S. P. de Visser, A. Altun, W. Thiel, *Chem. Rev.* **2005**, *105*, 2279–2328.
[49] In the reaction between $^5\mathbf{K}_{\mathbf{TMC(AN)}}$ and PR_3, the second electron shifts to π^*.
[50] D. Danovich, S. Shaik, *J. Am. Chem. Soc.* **1997**, *119*, 1773–1786.
[51] For some applications and generalizations in organometallic chemistry see: a) J. N. Harvey, M. Aschi, *Faraday Discuss.* **2003**, *124*, 129–143; b) R. Poli, J. N. Harvey, *Chem. Soc. Rev.* **2003**, *32*, 1–8; c) J. N. Harvey, *Phys. Chem. Chem. Phys.* **2007**, *9*, 331–343; d) S. Shaik, D. Danovich, D. Schröder, H. Schwarz, *Helv. Chim. Acta* **1995**, *78*, 1393–1407; e) D. Schröder, S. Shaik, H. Schwarz, *Acc. Chem. Res.* **2000**, *33*, 131–175; f) S. Shaik, H. Hirao, D. Kumar, *Acc. Chem. Res.* **2007**, *40*, 532–542.
[52] For considerations of blended reactivity in oxidation by FeO^+, see: M. Filatov, S. Shaik, *J. Phys. Chem. A* **1998**, *102*, 3835–3846.
[53] a) P. K. Sharma, S. P. de Visser, F. Ogliaro, S. Shaik, *J. Am. Chem. Soc.* **2003**, *125*, 2291–2300; b) S. P. de Visser, F. Ogliaro, Z. Gross, S. Shaik, *Chem. Eur. J.* **2001**, *7*, 5954–5960.
[54] a) See for example, the KIE in a similar process (H-migration) where the TS lies close in energy to the reactant. R. Schork, H. Köppel, *J. Chem. Phys.* **2001**, *115*, 7907–7923. b) Solvent relaxation has to be taken into account as well in the consideration of the barrier on the quintet state vis-à-vis the ZPE of the C–H vibration. Some of the solvent effect on the barrier is determined by polarization and has to be taken into account in such a consideration. However, the slow reorganization modes of the solvent are expected to follow after the molecular tunnel. This breakdown is not simple for the present computational data.
[55] S. P. de Visser, *J. Am. Chem. Soc.* **2006**, *128*, 9813–9824.

Received: November 5, 2007
Published online: January 9, 2008

